An Integrated Circuit With Transmit Beamforming Flip-Chip Bonded to a 2-D CMUT Array for 3-D Ultrasound Imaging

Ira O. Wygant, *Student Member, IEEE*, Nafis S. Jamal, *Student Member, IEEE*, Hyunjoo J. Lee, *Student Member, IEEE*, Amin Nikoozadeh, *Student Member, IEEE*, Ömer Oralkan, *Member, IEEE*, Mustafa Karaman, *Member, IEEE*, and Butrus T. Khuri-Yakub, *Fellow, IEEE*

***Abstract*—State-of-the-art 3-D medical ultrasound imaging requires transmitting and receiving ultrasound using a 2-D array of ultrasound transducers with hundreds or thousands of elements. A tight combination of the transducer array with integrated circuitry eliminates bulky cables connecting the elements of the transducer array to a separate system of electronics. Furthermore, preamplifiers located close to the array can lead to improved receive sensitivity. A combined IC and transducer array can lead to a portable, high-performance, and inexpensive 3-D ultrasound imaging system. This paper presents an IC flip-chip bonded to a 16 × 16-element capacitive micromachined ultrasonic transducer (CMUT) array for 3-D ultrasound imaging. The IC includes a transmit beamformer that generates 25-V unipolar pulses with programmable focusing delays to 224 of the 256 transducer elements. One-shot circuits allow adjustment of the pulse widths for different ultrasound transducer center frequencies. For receiving reflected ultrasound signals, the IC uses the 32-elements along the array diagonals. The IC provides each receiving element with a low-noise 25-MHz-bandwidth transimpedance amplifier. Using a field-programmable gate array (FPGA) clocked at 100 MHz to operate the IC, the IC generated properly timed transmit pulses with 5-ns accuracy. With the IC flip-chip bonded to a CMUT array, we show that the IC can produce steered and focused ultrasound beams. We present 2-D and 3-D images of a wire phantom and 2-D orthogonal cross-sectional images (B-scans) of a latex heart phantom.**

I. Introduction

Real-time 3-D ultrasound imaging is an increasingly prevalent medical imaging technology in fields such as obstetrics [1], [2] and cardiology [3], [4]. In contrast to traditional 2-D ultrasound imaging systems, 3-D imaging systems can form 2-D image planes in any orientation relative to the ultrasound transducer array and can acquire volumetric images. These capabilities simplify image acquisition and aid making quantitative measurements based on the acquired images [3]. Furthermore, because 3-D images can be acquired quickly and analyzed offline, examinations with 3-D ultrasound take less time and are less dependent on the skill of the sonographer [2], [5].

A. Background

Early 3-D ultrasound imaging systems (e.g., [6]) used sparsely populated 2-D arrays or mechanically scanned 1-D arrays of ultrasound transducer elements to simplify the transmit and receive electronics. Modern systems, however, use fully populated 2-D arrays for better image quality. In general, arrays with more elements result in better image resolution, contrast, and SNR; commercial systems use arrays with thousands of elements [7]. The elements in the arrays are typically about one-half wavelength in length and width (150 μm at 5 MHz). Connecting to and processing the signals from the elements of a large 2-D array require sophisticated packaging and electronics.

System connection cables are too bulky for connecting each element of a hand-held transducer array to a separate system of electronics. Furthermore, the capacitance of long cables (commonly 100 pF/m [8]) degrades the receive sensitivity of 2-D transducer array elements, which have capacitance on the order of several picofarads.

Incorporating some of the system's electronics into the hand-held probe results in fewer cables and better receive sensitivity. Furthermore, a compact connection between the array and integrated circuitry can result in a highly portable and inexpensive 3-D ultrasound imaging system. Such a system would enable wider use of 3-D ultrasound imaging, particularly because portability and cost, along with real-time imaging, are key advantages of ultrasound imaging compared with other common medical imaging modalities such as magnetic resonance imaging (MRI) and computed tomography (CT).

The electronics of a phased array 3-D ultrasound imaging system use the transducer array to steer a focused beam of ultrasound over the volume being imaged, and to detect the resulting reflected ultrasound. To generate a focused beam of ultrasound, a transmit beamformer provides each transmitting array element with a high-voltage pulse, or a series of coded pulses. The pulses are delayed relative to each other to create a beam of ultrasound steered in the direction of a focal point. A transmit beamformer that

Manuscript received October 16, 2008; accepted June 30, 2009. This work was supported by NIH grant CA99059. Work was performed in part at the Stanford Nanofabrication Facility (a member of the National Nanotechnology Infrastructure Network) which is supported by the National Science Foundation under Grant ECS-9731293.

I. O. Wygant, N. S. Jamal, H. J. Lee, A. Nikoozadeh, Ö. Oralkan, and B. T. Khuri-Yakub are with the Edward L. Ginzton Laboratory, Stanford University, Stanford, CA (e-mail: iwygant@stanford.edu).

M. Karaman is with the Electronics Engineering Department, Işik University, Istanbul, Turkey.

Digital Object Identifier 10.1109/TUFFC.2009.1297

accommodates high-voltage pulses (ideally 100 V or more [9]) and uses more elements of the transducer array results in better image SNR, with the limitation that peak ultrasound pressures and average ultrasound intensities cannot surpass government-mandated limits [10]–[12]. The accuracy of the transmit beamformer's delays impacts the sidelobe levels of the transmitted beams [13], [14]. Simulations of a specific imaging system's image of a point reflector [15], referred to as the point spread function, give precise indications of how delay quantization and delay uncertainty impact image quality.

The receiving electronics of a 3-D imaging system include preamplifiers, time-gain-compensation (TGC) amplifiers, and a receive beamformer. The preamplifiers should amplify the transducer signal while adding as little noise as possible to the input-referred noise of the transducer [16]. For 2-D array elements, which have a high impedance, the preamplifiers should be closely located to the array elements. TGC amplifiers equalize the echoes received from objects at different distances from the transducer by providing gain that increases with time for each received signal. A receive beamformer delays and coherently adds the received signals from different array elements to create a focused beam. To increase the frame rate for 3-D imaging, the transmitted beams may be defocused to create wider beams, in which case the receive beamformer creates several focused beams per transmitted beam [17], [18]. Analog-to-digital converters (ADCs) convert the focused beams to digital signals for further processing and display. In systems with relatively few receiving elements (e.g., 2-D imaging systems) the detected echoes can be converted to digital signals before receive beamforming. However, for large 2-D arrays, providing ADCs to every element is not practical.

Because 2-D transducer array elements are tightly packed together, electronics must connect to the array elements from the back side. Frequently this connection requires a specially designed connector to join pads on the back side of the transducer array with the pads of a flexible circuit board or an integrated circuit [19]–[25]. Alternatively, micromachined or polymer-based transducer technologies allow for the direct fabrication of the transducer array on an integrated circuit [26]–[30]. However, these methods generally require compromises in transducer fabrication methods. We directly flip-chip bond micromachined transducer arrays with through-wafer interconnects to an IC [31].

The literature contains numerous integrated circuit designs for ultrasound imaging systems. These studies include transmit beamformers [32], [33], analog receive beamformers [34]–[38], ADCs [39], and complete imaging systems [40]. High-voltage switch arrays for multiplexing have also been studied for multiplexing numerous transducer array elements over a fixed number of transmit and receive electronic channels [29], [41], [42].

In [31], we have described an IC flip-chip bonded to a 2-D transducer array for 3-D imaging. With that device, we demonstrated 100% element yield, good receive sensitivity, and a reliable means of flip-chip bonding a 2-D capacitive micromachined ultrasonic transducer (CMUT) array with through-wafer interconnects to an IC. The IC presented in [31] provided a pulser and preamplifier to every transducer element but only a single element could be used at a time for transmit and receive. As a result, we used classic synthetic aperture imaging, which suffers from lower SNR, higher grating lobes, and motion artifacts compared with conventional phased array imaging.

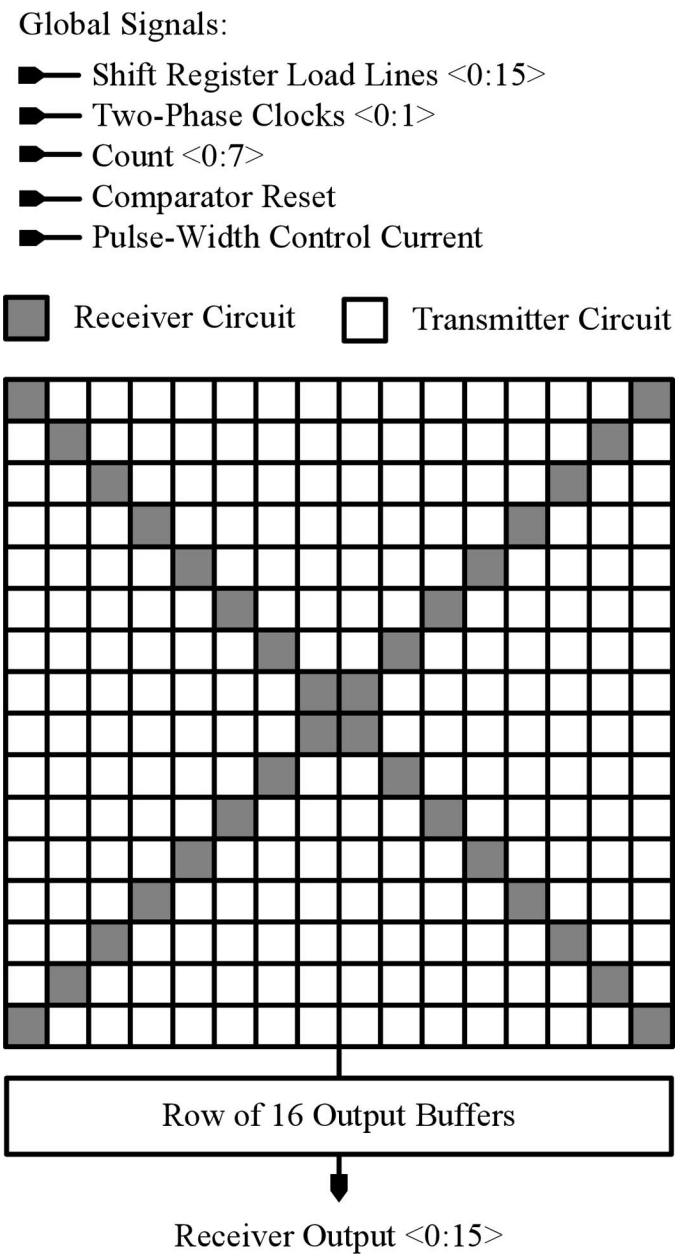

Fig. 1. Top-level diagram of the IC. The IC is designed to be flip-chip bonded to a 16 × 16-element ultrasound transducer array. It provides a 25-V pulser circuit to each of the 224 transmitting elements and a low-noise preamplifier to each of the 32 receiving elements. A control signal enables 16 receivers at a time for output on 16 signal lines.

B. Device Overview

In this paper, we present the design and testing of an IC that uses a 16 × 16-element transducer array for 3-D

TABLE I. IC DESIGN PROPERTIES.

Parameter	Single-Channel [31]	16-Channel
Array size	16 × 16	16 × 16
Transmit elements	256	224
Receive elements	256	32
Pulse voltage	25 V	25 V
Amplifier transimpedance gain	430 kΩ	215 kΩ
Amplifier bandwidth	10 MHz	25 MHz
Simultaneous active transmit elements	1	224
Simultaneous active receive elements	1	16
Power per receive channel	9 mW	9 mW

ultrasound imaging. We designed the IC for an intracavital ultrasound imaging application. However, the design could be extended to use larger arrays for other ultrasound imaging applications. The IC comprises a 224-element transmit beamformer and 32 preamplifiers. The transmit beamformer provides each of 224 of the 256 transducer elements with a 25-V pulser, a one-shot circuit, and an 8-bit shift register. A field-programmable gate array (FPGA) loads new focusing delay values into the shift registers for each new transmit beam focus. For receiving, the IC provides a transimpedance preamplifier to each of the 32 elements along the array diagonals. A previous study [43] showed that using the array diagonals for receiving gives acceptable imaging performance with a reduced number of receive channels. Dividing the array into transmit-only and receive-only elements simplifies the receive circuitry by eliminating the need for protection circuitry.

With this IC, we demonstrate the integration of the transmitting electronics, receiving electronics, and transducer array into a compact device. Compared with previously reported transmit beamformers [32], [33], the transmit beamformer presented here provides a much larger number of pulsers; these pulsers have a relatively high voltage and are compact enough to be used in arrays with thousands of elements. Fully packaged intracavital or endoscopic imaging probes have been demonstrated (e.g., [44]); these demonstrations include probes with 2-D transducer arrays for 3-D imaging [45], [46]. In [44], a custom-designed IC is closely associated with the transducer array. Here we show an IC for 3-D imaging that comprises more of the imaging system's functionality. Compared with the IC we describe in [31], the IC described in this paper uses many more elements in parallel for any single transmit and receive event, which results in significantly improved SNR and contrast. Table I compares the key features of the 2 ICs.

In this paper and in [31] we use CMUT arrays. CMUTs are ultrasound transducers manufactured using MEMS technology. They compete with piezolectric transducer technology for medical imaging [47], [48]. At present, medical imaging is dominated by piezoelectric transducer technology; the advantages of piezoelectric transducers include good transmit sensitivity (Pa/V) and a well-established manufacturing process. CMUTs provide wide bandwidth, which translates to better axial resolution, and benefit from MEMS fabrication processes that provide design flexibility, tight control over dimensions, and batch fabrication. For ring-shaped arrays or high-frequency arrays, the manufacturing advantages of CMUTs are particularly important [49], [50]. The capability of incorporating through-wafer interconnects [51], [52] with the CMUT array allows the array to be directly flip-chip bonded to the IC.

II. CIRCUIT DESIGN AND IMPLEMENTATION

We designed the IC for a high-voltage process (National Semiconductor, Santa Clara, CA) that provides bipolar, double diffused MOS (DMOS), and low- and high-voltage CMOS devices. The process provides a single poly layer and 2 metal layers. We chose this process because it provides high-voltage CMOS devices for the pulser circuitry. The process has a relatively large minimum feature size of 1.5 μm, which means that standard implementations of some circuits occupy large areas. As a result, circuit size was an important design consideration.

The IC interfaces 224 of the array elements for transmitting; it interfaces with the remaining 32 elements along the array diagonals for receiving (Fig. 1). It thus provides each element of the array with either a transmit circuit or a preamplifier. The transmit pulser circuit uses a 25-V supply. The remaining circuitry uses a 5-V supply.

The transmit circuit consists of an 8-bit shift register, a comparator, a one-shot, and a 25-V pulser (Fig. 2). For each new transmit beam, the FPGA-based imaging system that operates the IC loads 8-bit focusing delay values into every shift register. To transmit the beam, the imaging system increments an 8-bit Gray-code counter from one to the number of unique firing times. If, for example, every element has a unique firing time, then the counter increments from 1 to 224. Each transmit circuit's pulser fires when the value stored in its shift register is equal to the Gray-code counter. With this method of triggering the pulsers, which is similar to the method described in [32], the IC can transmit single pulses of arbitrarily steered and focused ultrasound.

The shift registers [Fig. 3(a)] for each row of 14 transducer elements connect in series. Sixteen input signals from the imaging system load the 16 rows of shift registers in parallel. Because the shift registers are loaded before each new transmit beam, their load time potentially re-

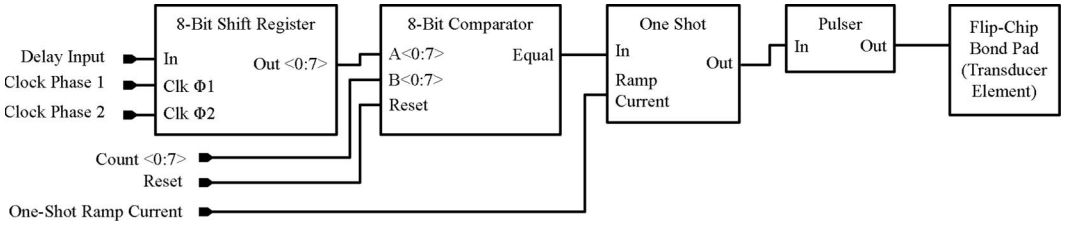

Fig. 2. Block diagram of the transmit circuit. Each transmit circuit generates a 25-V pulse when the value stored in its 8-bit shift register is equal to a global counter. For each new focal point, field-programmable gate array loads new delay values into the shift registers and increments a Gray-code counter from 0 to the number of unique pulser firing times.

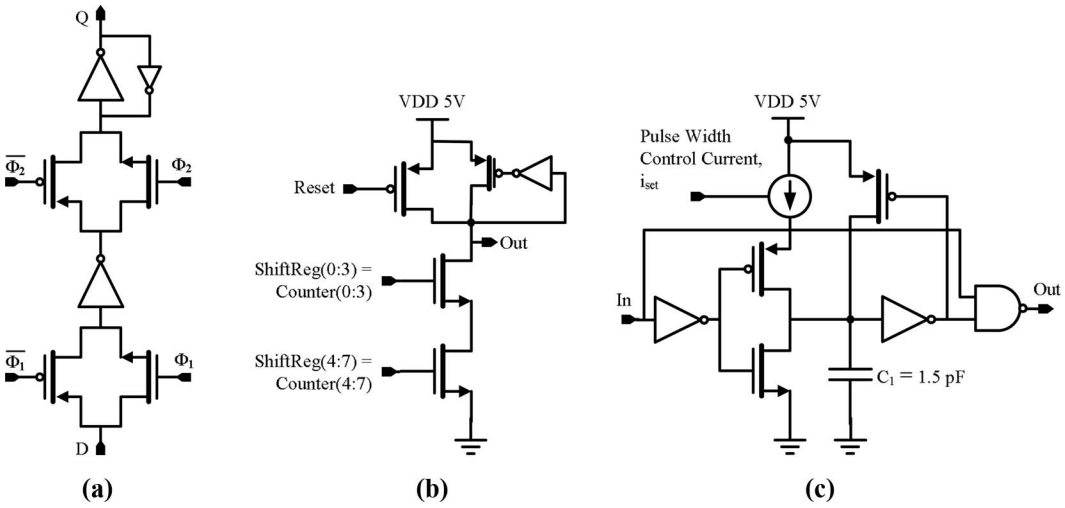

Fig. 3. Key transmit and receive circuits. Low transistor-count circuitry saves die area. (a) The shift register. A transmission-gate register stores transmit delay information. (b) The comparator. Dynamic logic saves die area and enables a simple one-shot implementation. (c) The one-shot circuit. A reference current determines the transmit pulse width.

TABLE II. EQUIVALENT CIRCUIT COMPONENT VALUES.

Parameter	Unit	Definition	Value
P	Pa	Impinging ultrasound pressure	
A	m^2	Equivalent parallel-plate area	9.1×10^{-9}
R_{rad}	Rayl·m^2	Radiation resistance	5.0×10^{-3}
L_{rad}	kg	Radiation inductance	1.8×10^{-11}
L_m	kg	Equivalent mass	1.2×10^{-11}
$1/C_m$	N/m	Equivalent spring constant	7.4×10^{4}
n	N/V	Transformer ratio	8.8×10^{-5}
C_0	pF	Device capacitance	0.3
C_p	pF	Estimated parasitic capacitance	0.5

duces the imaging frame rate; thus, their load time should be small compared with the pulse-echo time of the ultrasound beam. We assume an imaging depth of more than 3 cm, which corresponds to a pulse-echo time of more than 40 μs. We designed the registers for a load rate greater than 100 MHz. At 100 MHz, the load time for all 224 shift registers is 1.1 μs, which is negligible compared with the pulse-echo time.

In each transmit circuit, when the value stored in the shift register equals the Gray-code counter provided by the imaging system, the comparator's output goes high. The comparator [Fig. 3(b)] uses dynamic logic that is reset before each beam transmission. Dynamic logic helps make the comparator's size small. Additionally, because the output of the comparator stays high until the dynamic logic is reset, we can use a simple XOR implementation of the one-shot.

The one-shot drives the pulser and thus dictates the length of the pulse applied to the transducer element. The one-shot's output goes low for a time proportional to C_1/i_{set}. The current i_{set} is an adjustable current referenced with current mirrors to an off-chip current source. Every one-shot has the same i_{set}. Adjusting i_{set} allows the pulse length to be adjusted for a particular transducer's frequency response—transducers operating at higher frequencies require shorter pulses. In simulation, for i_{set} between 2

and 1 mA, the one-shot produced pulse widths between 70 ns and 150 ns, which are suitable for frequencies up to about 7 MHz.

The one-shot triggers the pulser circuit, which is the same pulser circuit we used in [31] and which we adapted from the circuit described in [53]. We sized the pulser to drive a load of 2 pF. In simulation, for a 25-V pulse, the pulser had a rise time of 20 ns and a fall time of 16 ns. The corresponding slew rates were 1,000 and 1,300 MV/sec.

For design of the preamplifier, we modeled the CMUT using its equivalent circuit [Fig 4(a)]. Finite element modeling and analytical expressions for the CMUT's response to pressure and voltage are used to obtain circuit parameter values for the model [54]–[56].

The equivalent circuit is derived so that circuit elements on the left side represent mechanical properties; on this side, voltage represents force and current represents velocity. Circuit elements on the right side of the transformer represent electrical properties of the CMUT. Table II defines the components of the equivalent circuit and gives component values for a 250 × 250 μm CMUT array element like those used in this study.

For the circuit design, we can simplify the CMUT equivalent circuit model. Because the circuit is heavily damped and we are most interested in the CMUT's properties close to its center frequency, we can assume the mechanical impedances and spring softening capacitor are close to resonance and thus ignore L_m, C_m, and $-C_0$. With these assumptions, the equivalent circuit becomes a capacitive current source [Fig. 4(b)].

This simple model shows that for a given echo pressure, the current produced by the CMUT element is proportional to the CMUT element's area and its sensitivity, quantified by n. Because n and R_{rad} are both proportional to area, the CMUT's short-circuit current is proportional to its area. If the preamplifier noise dominates the thermal noise of the transducer, then for a given echo pressure, the SNR increases with the CMUT's area because the signal current increases with area. If the thermal noise of the radiation resistance dominates, then the SNR increases with the square root of the area because the signal current increases with area and the noise current increases with the square root of the area.

For a fixed area, increasing n, e.g., by increasing the dc bias voltage, also increases the signal current. For the preamplifier-noise dominated case, increasing n improves the SNR. For the thermal-noise dominated case, increasing n does not affect the SNR. However, it increases the magnitude of the electrical-referred noise resulting in a lower noise figure for a fixed input-referred preamplifier noise.

For this study, our model of a CMUT element has an equivalent parallel resistance of 1 MΩ and a parallel capacitance of 0.26 pF. We also included a parallel parasitic capacitor. In [31], we measured total parasitic capacitance between 100 and 500 fF associated with a 250 × 250 μm CMUT element's through-wafer interconnect, bottom electrode, and flip-chip bond pad. To accommodate variations in device capacitance and parasitic capacitance, we designed the preamplifier and pulser assuming a combined device and parasitic capacitance of 2 pF.

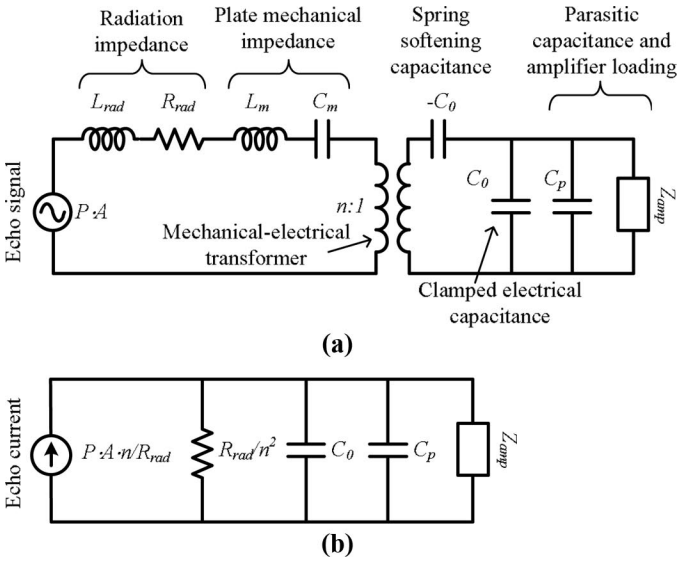

Fig. 4. An equivalent circuit model represents the transducer elements for the preamplifier design. Except for C_p, R_{load}, and the radiation impedance, the circuit components scale with the transducer element size. As the element size increases relative to a wavelength, the radiation impedance approaches $R_{\text{med}} \cdot A$, where R_{med} equals 1.5 MRayls for water. (a) The complete circuit model. (b) At the transducer's center frequency in immersion, R_{rad} dominates L_{rad}, R_{loss}, L_m, and C_m. Thus, the equivalent circuit simplifies to a current source in parallel with a resistor and capacitor.

The IC provides a dedicated transimpedance amplifier (Fig. 5) to each of the 32 receiving array elements [57]. The amplifier consists of a simple common source amplifier, a source follower buffer, and a 215-kΩ feedback resistor. In simulation, the open-loop common source amplifier has a gain of 100 and a gain-bandwidth product of about 900 MHz. The closed loop transimpedance amplifier has a transimpedance gain of 215 kΩ and a bandwidth of 25 MHz.

The 2 amplifiers for each column of elements share a single p-type source-follower output buffer. We designed the output buffer to drive capacitive loads as large as 50 pF and to have at least an 800-mV peak-to-peak output swing (determined using the 1-dB compression point) for frequencies up to 10 MHz. The buffer can drive the capacitance of a short cable connecting the IC's output with supporting electronics. However, driving the several meters of cable between a hand-held probe and imaging system would require additional off-chip buffers. However, off-chip buffers have the benefit they can have high drive-capability and be located away from the transducer array, where power consumption and heat dissipation are less critical.

Power consumption is an important parameter for the IC because power consumed by the IC heats the transducer array, the temperature of which must be kept within safe limits for contact with a person. For a precise prediction of power consumption limits, a thermal model of the

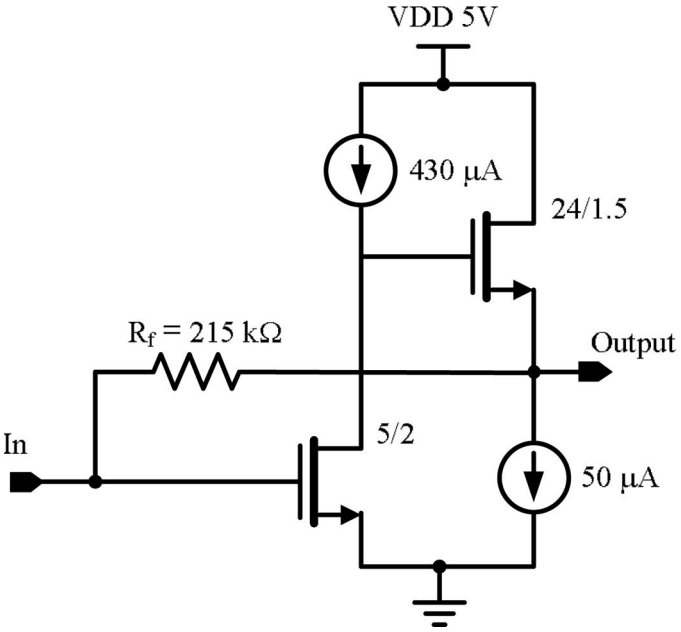

Fig. 5. Transimpedance amplifiers located directly beneath the receiving transducer elements amplify the received signals.

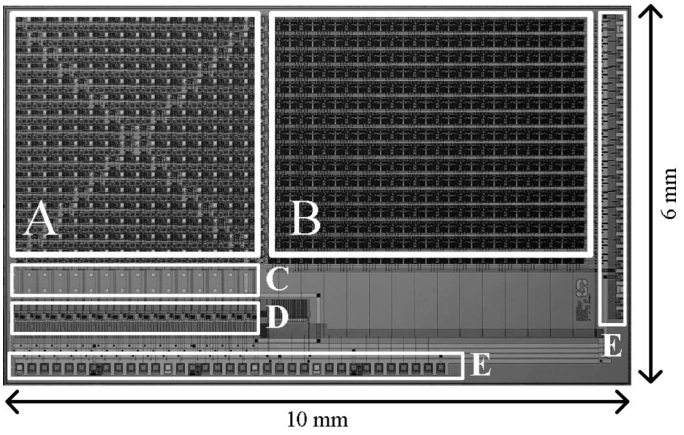

Fig. 6. A photograph of the IC. (a) A 16 × 16-array of flip-chip bond pads, 224 pulsers, and 32 receivers, (b) Shift register and comparator array, (c) CMUT dc-bias pads, (d) output buffers, (e) wire-bond pads.

probe [58], [59] can be used to estimate heating of the probe and surrounding tissue. We targeted a power consumption of 150 mW, which we divided equally between the preamplifier and buffer. Our 150 mW power budget is greater than the 100 mW upper limit given in [44] for a 1.83-mm diameter invasive ultrasound imaging probe. However, the IC presented here is much larger than the IC described in [44]; thus, it has lower power density and provides more area for heat dissipation.

For layout of the IC we divided the transmit and receive circuitry into 2 parts (Fig. 6). An array of 16 × 16 flip-chip bond pads occupies the left side of the IC. The flip-chip bond pads are 50-μm squares of top-level aluminum and have a pitch of 250 μm. One-shots and pulsers surround the flip-chip bond pads for transmitting elements. Preamplifiers surround the flip-chip bond pads for receiving elements. The right side of the IC consists of

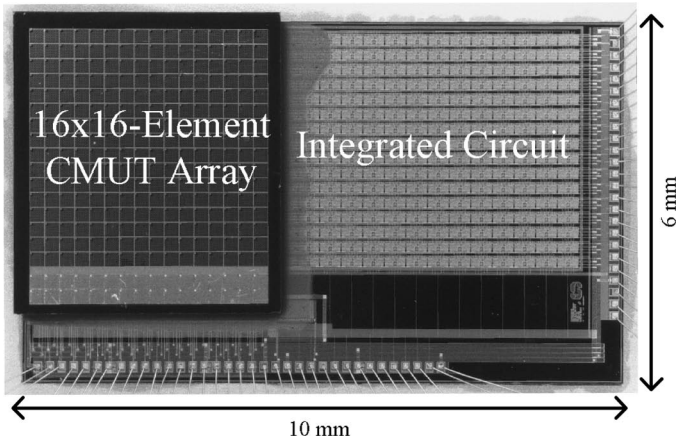

Fig. 7. Photograph of the transducer array flip-chip bonded to the IC. All 256 transducer elements are functional in the flip-chip bonded device.

a 16 × 14 array of shift registers and comparators. Two rows of flip-chip bond pads on the bottom left provide the dc bias voltage required by the CMUT. The dc bias circuit is illustrated in [31]. We kept the left and top sides of the IC free of wire bond pads to provide the possibility of tiling 4 flip-chip bonded arrays together to form a 32 × 32-element array.

III. Testing

We tested the IC on its own and flip-chip bonded to a 2-D CMUT array (Fig. 7). In both cases, we packaged the device in a 121-pin PGA (pin grid array) package. A printed circuit board provided reference currents, off-chip output buffers, and digital level shifters for the IC. Digital signals for the IC were generated by a PC hosting an FPGA-based data acquisition and signal processing system (VHS-ADC, Lyrtech Signal Processing, Quebec, Canada). This system can transfer data between the PC and FPGA (Virtex II XC2V6000, Xilinx, Inc., San Jose, CA) over the PC's cPCI bus at rates of up to about 50 MB/s.

For each new transmit beam, the PC transfers data to the FPGA. These data include values to load into the IC's shift registers and the number of clock cycles to wait between each increment of the Gray-code counter. The FPGA then loads the IC's shift registers and generates the 8-bit Gray-code counter values that trigger the IC's pulsers.

To observe the pulses generated by the IC's transmit circuits, we wire bonded the flip-chip bond pads of 14 transmit circuits to pins of the package. We used a low-capacitance active probe (1156A Active Probe, Agilent Technologies, Palo Alto, CA) to measure the pulses generated by the IC for various beam focal points (Fig. 8). To determine the jitter of the generated pulses, we measured the delay between the transition of the Gray-code counter generated by the FPGA and the pulse generated by the IC. For the 14 wire-bonded pulsers, we measured delays between 40 and 48 ns; the mean delay was 44 ns with a

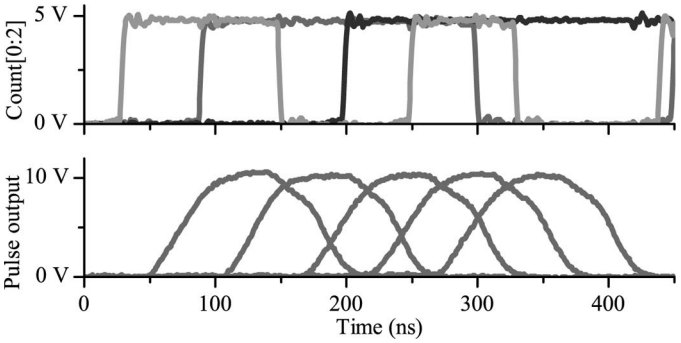

Fig. 8. The least 3 significant bits of the Gray-code counter and 5 measured pulser outputs. The top panel shows each bit of the counter with a different shade of gray. A pulser fires when the value stored in its shift register equals the global counter value. The pulser-circuit generates voltages as high as 25 V. For this measurement, we limited the pulser output voltage to 10 V to make the measurement with a low-capacitance active oscilloscope probe.

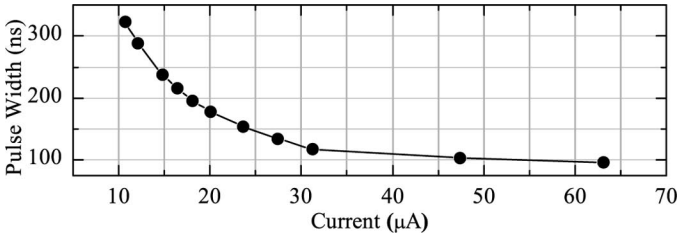

Fig. 9. One-shot pulse width as a function of an adjustable current provided off chip. The one-shot generates pulses as short as 100 ns.

standard deviation of 2.5 ns (1.3% of a period at 5 MHz). For a single pulser, the jitter between consecutive pulses was 440 ps, which indicates that most of the pulse delay variation comes from channel-to-channel variations in the comparator and one-shot circuits. Increasing the speed of the comparator circuit by using larger NMOS pulldown transistors would be one way of improving the jitter.

We also measured the pulse length channel-to-channel variation. For a mean pulse width of 95 ns, the 14 measured pulse lengths varied between 92.6 and 98.5 ns with a standard deviation of 2.1 ns. Although pulse-length variation impacts the image quality less than pulse-delay variation, it could be improved by increasing the size of the one-shot capacitor, which occupies about 1% of the total circuit area for a single element, and the size of the current mirrors. To achieve much better pulse uniformity, a clock signal should dictate the pulse lengths rather than a one-shot circuit.

For a 100-MHz FPGA clock, the mean error between the measured pulse delays and the ideal calculated pulse delays was 5 ns. Most of this error comes from the 10-ns FPGA clock period. For greater accuracy, we could use a higher FPGA clock rate; we tested the IC with FPGA clock rates up to the system's maximum rate of 125 MHz. As described in [32], a clock divider implemented on the IC would also give better timing resolution.

We measured the pulse width as a function of one-shot bias current (Fig. 9). The IC produced pulses as short as 100 ns, which is suitable for frequencies up to about 5 MHz. For a given bias current, the IC generated longer pulses than expected from simulation, which probably resulted from a larger than expected one-shot charge capacitor [C_1 in Fig. 2 or 3(c)] and parasitic capacitance. To accommodate a wider range of transducer operating frequencies, the one-shot should be designed to accommodate larger bias currents. Properly sized, the pulser circuit can generate pulses for high-frequency arrays; for the IC used in [49], we sized the pulser circuit to generate pulses for transducers with frequencies of up to 50 MHz.

Because the bandwidth of the transimpedance amplifier is sensitive to input capacitance and because it requires a high source impedance, it is difficult to measure its bandwidth electrically. A network analyzer is often used to characterize the frequency response of high-frequency transimpedance amplifiers. However, because the input impedance of the amplifier presented here is several kilohms, it is difficult to measure the S_{11} parameter needed to determine the gain. In [44], the authors included a test structure on the IC to measure the bandwidth. In this paper, because the simulated bandwidth significantly exceeds the frequency content of the transducers used for imaging, we assume that the amplifier's response did not impact the frequency content of the measured ultrasound echoes.

We tested the IC in combination with a CMUT array by flip-chip bonding a 16 × 16-element CMUT array to the IC. To prepare the IC for flip-chip bonding, an electroless plating process creates a 5-μm thick Ni/Au layer on the IC pads; a solder-jetting process then deposits 80-μm diameter solder balls on the pads (Pac Tech USA, Santa Clara, CA) [31]. To test the device in immersion, we attached a small plastic tank to the IC's PGA package and filled it with vegetable oil. Using vegetable oil in place of water enables us to test the device in immersion without having to electrically insulate the CMUT and IC. For testing in water, we have shown that parylene and polydimethylsiloxane (PDMS) effectively insulate the CMUT [60].

To test the functionality of each element and its corresponding electronics, we fired each element individually and recorded the echoes from the surface of the oil detected by the 32 receiving elements. We observed an echo for every transmitting and receiving element, which demonstrates the functionality of the IC and every element of the array.

To measure the focusing capability of the flip-chip bonded device, we transmitted beams with various focal points and measured the pressure at the focal point with a hydrophone. For a focal point at 4 mm on-axis from the center of the array, we measured a peak-to-peak pressure of 850 kPa, which is about 120 times the pressure produced by a single element in the center of the array (Fig. 10). At 4 mm, the focusing gain is less than 224 (the total number of transmitting elements) because those elements at the edge, which are at greater angles relative to the hydrophone, contribute less to the pressure at the focal point than those elements in the center. Moving the hydrophone

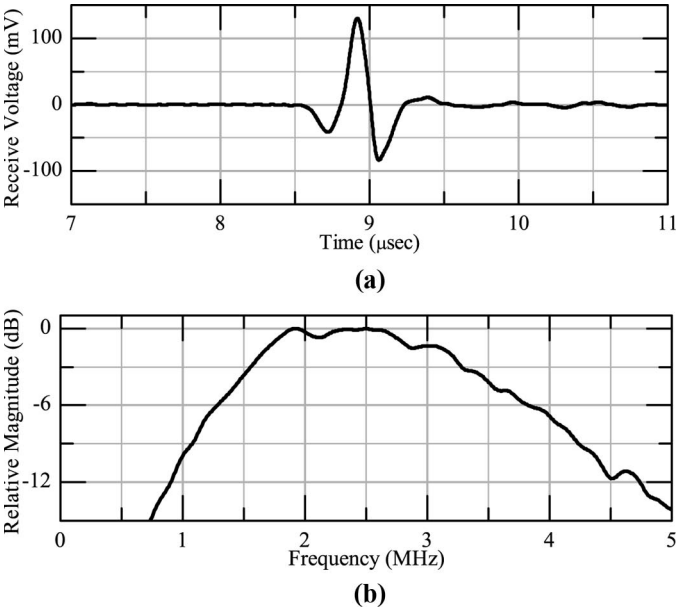

Fig. 10. We measured the pressure at a focal point located 4 mm on-axis from the array's center. (a) At the focal point, the transmitted pulses add together. For a center frequency of 2.2 MHz, the hydrophone output corresponds to 850 kPa peak-to-peak, which is about 120 times the pressure from a single element. (b) The Fourier transform of the measured signal at the focal point.

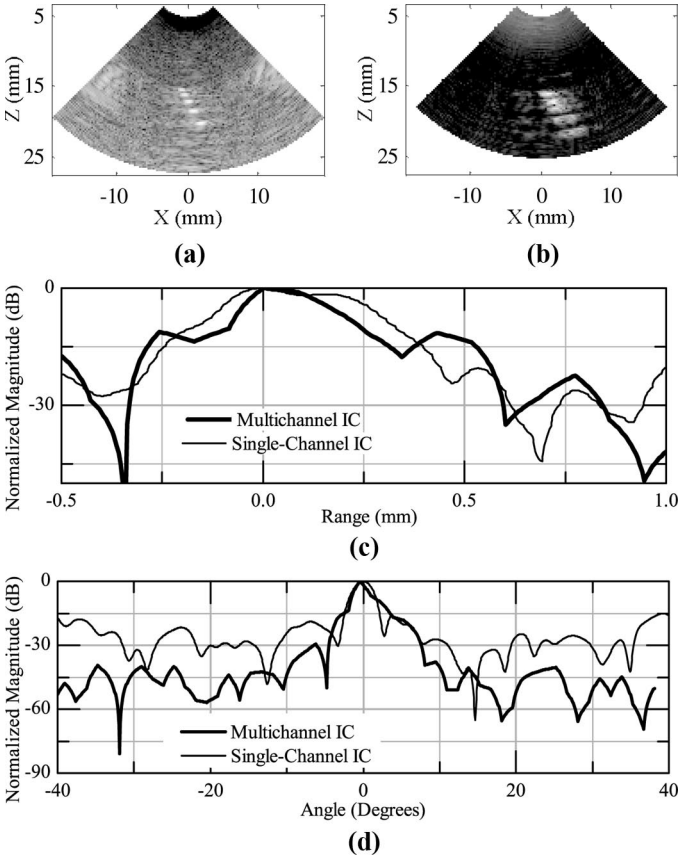

Fig. 11. Comparison between images of 5 fishing line segments acquired with the single-channel IC described in [31] and the IC described in this work. (a) Image from [31] acquired using 16 averages. (b) Image acquired using the IC described in this paper without averaging and using 60 beams spanning 90°. The transmit focus distance is 15 mm. We increased the spacing between the 2 closest lines from 0.8 to 1.2 mm for the multichannel-IC image; otherwise, the wire phantoms are identical. Both images have 50-dB dynamic range and a gamma value of 0.8. (c) Axial image profile aligned to the center line segment. (d) Lateral image profile aligned to the center line segment. The image acquired with the multichannel IC demonstrates significantly improved dynamic range with the capability of acquiring images at a much higher frame rate. A lower transducer frequency (2.2 MHz compared with 5.1 MHz) and the different transmit and receive array configuration [43] results in decreased resolution in the image acquired with the multichannel IC.

to distances further from the IC shows focusing gains approaching 224.

To determine the minimum detectable pressure for a combined CMUT element and preamplifier, we measured the electrical output noise and divided the result by the measured receive sensitivity. To determine receive sensitivity, we used a hydrophone to measure the pressure generated by a single element at a distance of 22.5 mm. We then measured the pulse-echo signal from the oil-air interface for a 2-way distance of 22.5 mm. The amplitude of the pulse-echo signal divided by the measured pressure equals the receive sensitivity assuming the oil-air interface is a perfect reflector. We measured the electrical noise at the output of the discrete buffer and amplifier that follow the IC's output using a spectrum analyzer (2712 Spectrum Analyzer, Tektronix, Beaverton, OR). At 4.4 MHz, we measured a 414 mV/kPa receive sensitivity and an output electrical noise of 380 nV/$\sqrt{\text{Hz}}$, which results in an input referred noise of 0.9 mPa/$\sqrt{\text{Hz}}$.

Changing the CMUT bias voltage, and thus the CMUT's sensitivity, results in negligible changes in the measured noise. This invariance indicates that electrical sources dominate the total noise. The noise of the 215-kΩ feedback resistor (280 fA/$\sqrt{\text{Hz}}$) dominates the noise of the transimpedance amplifier. Increasing the feedback resistor value, at the expensive of bandwidth, or using an amplifier topology with capacitive feedback are options for reducing the preamplifier noise.

To assess the imaging capability of the IC, we acquired images of a wire phantom constructed using 150-μm diameter fishing line. To acquire the images, we programmed the PC and FPGA system to generate the desired transmit beams. An FPGA-implemented real-time beamformer reconstructed the received data sampled at 100 MHz. The beamformer uses a standard delay-and-sum algorithm. Fig. 11 compares the acquired images with those obtained with the single-channel IC presented in [31]; Fig. 12 shows the volume-rendered image. The images obtained with no averaging have about 23 dB better SNR than those obtained using the single-channel IC using 16 averages. Based on the number of transmit and receive elements, we expect about a 26 dB improvement in SNR [43]. About 6.5 dB of improvement is offset by increased diffraction and attenuation losses at the CMUT array's lower center frequency (2.2 MHz compared with 5.1 MHz in [31]). However, the higher source pressure of the CMUT array used in this study compensates for the lost improvement.

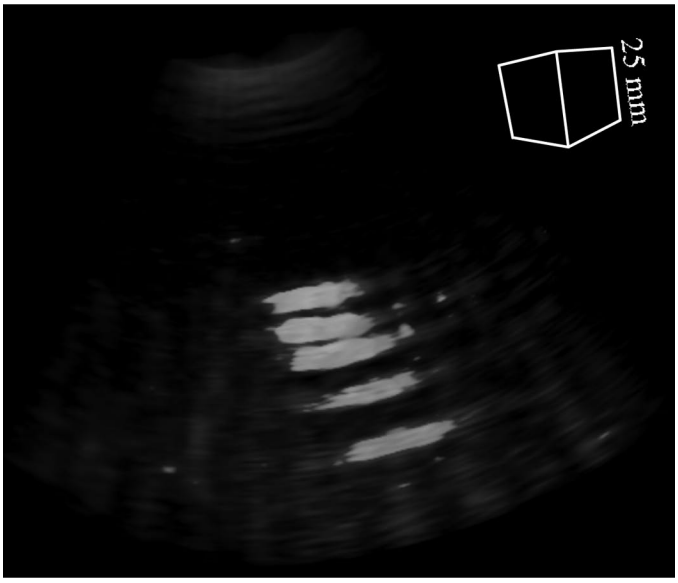

Fig. 12. Scan converted and rendered volume of five 150-μm diameter fishing line segments. The acquired volume spans 60° in the horizontal direction (32 beams) and 30° (16 beams) in the vertical direction. In the range direction, the volume extends from 5 to 25 mm. The image is shown with 40 dB of dynamic range. The first 25 dB of dynamic range has high transparency to prevent occlusion of the line segments.

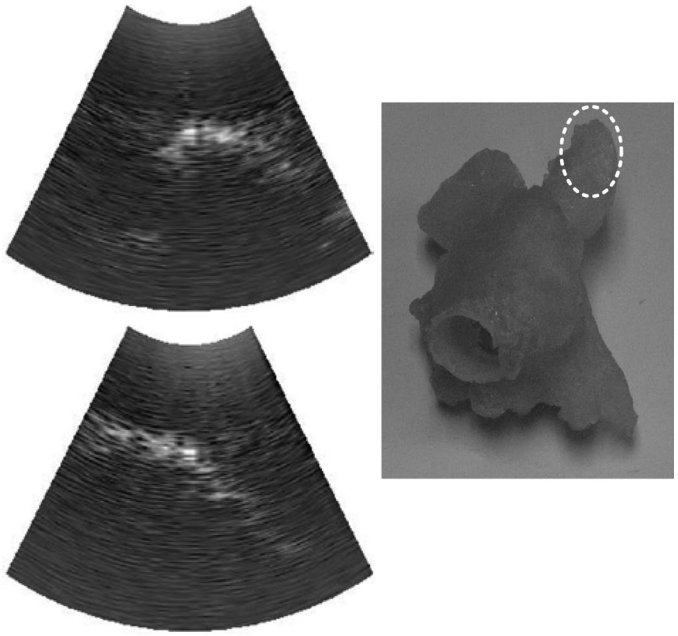

Fig. 14. Two orthogonal 2-D image cross sections of a left atrium heart phantom and a photograph of the phantom illustrating the imaged location. The ultrasound images have 25 dB dynamic range and a gamma value of 0.8. They span 60° and range from 10 to 25 mm.

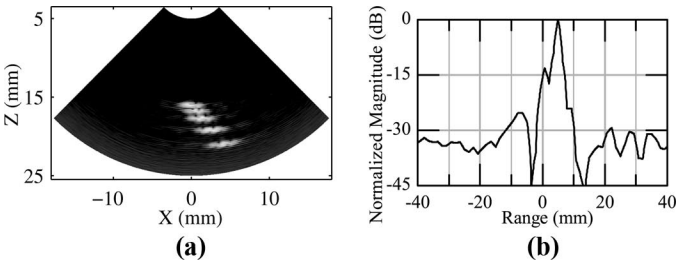

Fig. 13. Image acquired using only transmit beamforming. To assess the transmit beamforming capability of the IC, we acquired an image using all 224 transmit elements and a single receive channel. The imaging contains 64 beams that scan a 60° sector angle. (a) Image of a wire phantom shown with 30-dB dynamic range and a gamma value of 0.8. (b) Profile of the center wire.

With 16 averages, the single-channel IC requires 4096 transmits to obtain a full 3-D volume, which compares to about 1000 transmits for the multichannel IC. The multichannel IC also offers more ways of achieving high frame rates; for example, using defocused transmit beams or acquiring 2-D cross sections would increase the frame rate.

To separately evaluate the IC's transmit beamforming capability, we acquired an image using a single receive channel. Fig. 13 demonstrates that the IC transmits a focused beam of ultrasound. Finally, we acquired orthogonal 2-D cross-section images (B-scans) of a heart phantom (Fig. 14).

IV. Conclusion

The results presented in this paper demonstrate that the IC can transmit on all 224 elements with programmable delays and can be used to generate arbitrarily focused beams of ultrasound. Flip-chip bonded to a 256-element 2-D CMUT array, every transmit and receive element of the device is functional and can be used for 3-D imaging. For real-time imaging, we developed a real-time data acquisition and image reconstruction system. Assuming an imaging depth of 3 cm for intracavital imaging and the use of 40 × 40 transmit beams spanning 90° × 90°, up to 12 volumes per second could be acquired. Higher volume rates can be obtained by transmitting fewer defocused transmit beams or reducing the size of the image volume.

For improved SNR and for imaging techniques such as harmonic imaging, ultrasound systems are increasingly using coded excitation pulses [61]. To generate coded excitations, some of the pulsers would need to be retriggered while others are still firing, which is not possible with the dynamic logic comparator and one-shot circuit used for the IC presented here. Using retriggerable comparators and one-shots, which could have the drawback of consuming more area, the same general IC architecture could be used to transmit more complex waveforms.

In summary, the IC presented in this paper provides significantly better image SNR than the IC we demonstrated in [31]. In addition, it shows how a large number of transmit elements can be utilized with a minimal number of signal lines, which is a step toward a compact and integrated 3-D ultrasound imaging system.

Acknowledgment

National Semiconductor (Santa Clara, CA) fabricated the ICs and provided circuit design support. X. Zhuang

and S. Ergun fabricated the CMUT arrays for this work. Work was performed in part at the Stanford Nanofabrication Facility (a member of the National Nanotechnology Infrastructure Network) which is supported by the National Science Foundation under Grant ECS-9731293, its lab members, and the industrial members of the Stanford Center for Integrated Systems. Pac Tech USA, Inc. (Santa Clara, CA) provided solder-jetting and electroless Ni/Au bumping services. Dr. D. Sahn of the Oregon Health and Science University provided the heart phantom.

References

[1] L. F. Goncalves, W. Lee, J. Espinoza, and R. Romero, "Three- and 4- dimensional ultrasound in obstetric practice: Does it help?" *J. Ultrasound Med.*, vol. 24, no. 12, pp. 1599–1624, 2005.

[2] B. R. Benacerraf, T. D. Shipp, and B. Bromley, "Three-dimensional US of the fetus: Volume imaging," *Radiology*, vol. 238, no. 3, pp. 988–996, 2006.

[3] I. S. Salgo, "Three-dimensional echocardiographic technology," *Cardiol. Clin.*, vol. 25, no. 2, pp. 231–239, 2007.

[4] J. Hung, R. Lang, F. Flachskampf, S. K. Shernan, M. L. McCulloch, D. B. Adams, J. Thomas, M. Vannan, and T. Ryan, "3-D echocardiography: A review of the current status and future directions," *J. Am. Soc. Echocardiogr.*, vol. 20, no. 3, pp. 213–233, 2007.

[5] B. R. Benacerraf, T. D. Shipp, and B. Bromley, "Improving the efficiency of gynecologic sonography with 3-dimensional volumes: A pilot study," *J. Ultrasound Med.*, vol. 25, no. 2, pp. 165–171, 2006.

[6] S. W. Smith, H. R. Pavy, and O. T. von Ramm, "High-speed ultrasound volumetric imaging system. I. Transducer design and beam steering," *IEEE Trans. Ultrason. Ferroelectr. Freq. Control*, vol. 38, no. 2, pp. 100–108, 1991.

[7] L. F. Goncalves, J. Espinoza, J. P. Kusanovic, W. Lee, J. K. Nien, J. Santolaya-Forgas, G. Mari, M. C. Treadwell, and R. Romero, "Applications of 2-dimensional matrix array for 3- and 4-dimensional examination of the fetus: A pictorial essay," *J. Ultrasound Med.*, vol. 25, no. 6, pp. 745–755, 2006.

[8] Precision Interconnect, "MODULUS3 cable assemblies data sheet," Berwyn, PA, 2004.

[9] B. Haider, "Power drive circuits for diagnostic medical ultrasound," in *2006 IEEE Int. Symp. Power Semiconductor Devices and ICs*, 2006, pp. 1–8.

[10] U.S. Department of Health and Human Services Food and Drug Administration, Center for Devices and Radiological Health, "Information for manufacturers seeking marketing clearance of diagnostic ultrasound systems and transducers," U.S. Department of Health and Human Services, Washington, DC, 1997.

[11] NEMA, "Standard for real-time display of thermal and mechanical acoustic output indices on diagnostic ultrasound equipment," National Electrical Manufacturers Association, Rosslyn, VA, 2004.

[12] J. G. Abbott, "Rationale and derivation of MI and TI—A review," *Ultrasound Med. Biol.*, vol. 25, no. 3, pp. 431–441, 1999.

[13] D. K. Peterson and G. S. Kino, "Real-time digital image reconstruction: A description of imaging hardware and an analysis of quantization errors," *IEEE Trans. Sonics Ultrason.*, vol. 31, no. 4, pp. 337–351, 1984.

[14] S. Holm and K. Kristoffersen, "Analysis of worst-case phase quantization sidelobes in focused beamforming," *IEEE Trans. Ultrason. Ferroelectr. Freq. Control*, vol. 39, no. 5, pp. 593–599, 1992.

[15] J. Jensen, "Field: A program for simulating ultrasound systems," *Med. Biol. Eng. Comput.*, vol. 34, pp. 351–353, 1996.

[16] T. L. Rhyne, "Characterizing ultrasonic transducers using radiation efficiency and reception noise figure," *IEEE Trans. Ultrason. Ferroelectr. Freq. Control*, vol. 45, no. 3, pp. 559–566, 1998.

[17] D. P. Shattuck, M. D. Weinshenker, S. W. Smith, and O. T. von Ramm, "Explososcan: A parallel processing technique for high speed ultrasound imaging with linear phased arrays," *J. Acoust. Soc. Am.*, vol. 75, no. 4, pp. 1273–1282, 1984.

[18] O. T. von Ramm, S. W. Smith, and H. R. Pavy, "High-speed ultrasound volumetric imaging system. II. Parallel processing and image display," *IEEE Trans. Ultrason. Ferroelectr. Freq. Control*, vol. 38, no. 2, pp. 109–115, 1991.

[19] M. Greenstein, P. Lum, H. Yoshida, and M. Seyed-Bolorforosh, "A 2.5 MHz 2-D array with Z-axis backing," in *Proc. 1996 IEEE Ultrasonics Symp.*, vol. 2, 1996, pp. 1513–1516.

[20] R. E. Davidsen and S. W. Smith, "Two-dimensional arrays for medical ultrasound using multilayer flexible circuit interconnection," *IEEE Trans. Ultrason. Ferroelectr. Freq. Control*, vol. 45, no. 2, pp. 338–348, 1998.

[21] S. W. Smith and E. D. Light, "Two-dimensional array transducers using thick film connection technology," *IEEE Trans. Ultrason. Ferroelectr. Freq. Control*, vol. 40, no. 6, pp. 727–734, 1993.

[22] L. Daane and M. Greenstein, "A demountable interconnect system for a 50×50 ultrasonic imaging transducer array," *IEEE Trans. Ultrason. Ferroelectr. Freq. Control*, vol. 44, no. 5, pp. 978–982, 1997.

[23] J. O. Fiering, P. Hultman, W. Lee, E. D. Light, and S. W. Smith, "High-density flexible interconnect for two-dimensional ultrasound arrays," *IEEE Trans. Ultrason. Ferroelectr. Freq. Control*, vol. 47, no. 3, pp. 764–770, 2000.

[24] B. Savord and R. Solomon, "Fully sampled matrix transducer for real time 3-D ultrasonic imaging," in *2003 IEEE Symp. Ultrasonics*, vol. 1, 2003, pp. 945–953.

[25] W. Lee, S. Idriss, P. Wolf, and S. Smith, "A miniaturized catheter 2-D array for real-time, 3-D intracardiac echocardiography," *IEEE Trans. Ultrason. Ferroelectr. Freq. Control*, vol. 51, no. 10, pp. 1334–1346, 2004.

[26] P. C. Eccardt and K. Niederer, "Micromachined ultrasound transducers with improved coupling factors from a CMOS compatible process," *Ultrasonics*, vol. 38, no. 1-8, pp. 774–780, 2000.

[27] R. Noble, R. Davies, M. Day, L. Koker, D. King, K. Brunson, A. Jones, J. McIntosh, D. Hutchins, T. Robertson, and P. Saul, "Cost-effective and manufacturable route to the fabrication of high-density 2-D micromachined ultrasonic transducer arrays and (CMOS) signal conditioning electronics on the same silicon substrate," in *2001 IEEE Ultrasonics Symp.*, vol. 2, 2001, pp. 941–944.

[28] Y. Mo, T. Tanaka, K. Inoue, K. Yamashita, and Y. Suzuki, "Front-end processor using BBD distributed delay-sum architecture for micromachined ultrasonic sensor array," *J. Microelectromech. Syst.*, vol. 12, no. 4, pp. 506–512, 2003.

[29] C. Daft, S. Calmes, D. da Graca, K. Patel, P. Wagner, and I. Ladabaum, "Microfabricated ultrasonic transducers monolithically integrated with high voltage electronics," in *2004 IEEE Ultrasonics Symp.*, vol. 1, 2004, pp. 493–496.

[30] C. Daft, P. Wagner, B. Bymaster, S. Panda, K. Patel, and I. Ladabaum, "cMUTs and electronics for 2-D and 3-D imaging: monolithic integration, in-handle chip sets and system implications," in *2005 IEEE Ultrasonics Symp.*, vol. 1, 2005, pp. 463–474.

[31] I. Wygant, X. Zhuang, D. Yeh, O. Oralkan, A. Ergun, M. Karaman, and B. Khuri-Yakub, "Integration of 2-D CMUT arrays with front-end electronics for volumetric ultrasound imaging," *IEEE Trans. Ultrason. Ferroelectr. Freq. Control*, vol. 55, no. 2, pp. 327–342, 2008.

[32] J. V. Hatfield and K. S. Chai, "A beam-forming transmit ASIC for driving ultrasonic arrays," *Sens. Actuators A*, vol. 92, no. 1-3, pp. 273–279, 2001.

[33] I. G. Mina, H. Kim, I. Kim, S. K. Park, K. Choi, T. N. Jackson, R. L. Tutwiler, and S. Trolier-McKinstry, "High frequency piezoelectric MEMS ultrasound transducers," *IEEE Trans. Ultrason. Ferroelectr. Freq. Control*, vol. 54, no. 12, pp. 2422–2430, 2007.

[34] T. Halvorsrod, W. Luzi, and T. S. Lande, "A log-domain μbeamformer for medical ultrasound imaging systems," *IEEE Trans. Circuits Syst. I, Regul. Pap.*, vol. 52, no. 12, pp. 2563–2575, 2005.

[35] B. Stefanelli, I. O'Connor, L. Quiquerez, A. Kaiser, and D. Billet, "An analog beam-forming circuit for ultrasound imaging using switched current delay lines," *IEEE J. Solid-State Circuits*, vol. 35, no. 2, pp. 202–211, 2000.

[36] M. Yaowu, T. Tanaka, S. Arita, A. Tsuchitani, K. Inoue, and Y. Suzuki, "Pipelined delay-sum architecture based on bucket-brigade devices for on-chip ultrasound beamforming," *IEEE J. Solid-State Circuits*, vol. 38, no. 10, pp. 1754–1757, 2003.

[37] J. R. Talman, S. L. Garverick, and G. R. Lockwood, "Integrated circuit for high-frequency ultrasound annular array," in *Proc. 2003 IEEE Custom Integrated Circuits Conf.*, 2003, pp. 477–480.

[38] J. R. Talman, S. L. Garverick, C. E. Morton, and G. R. Lockwood, "Unit-delay focusing architecture and integrated-circuit implementation for high-frequency ultrasound," *IEEE Trans. Ultrason. Ferroelectr. Freq. Control*, vol. 50, no. 11, pp. 1455–1463, 2003.

[39] K. Kaviani, O. Oralkan, P. Khuri-Yakub, and B. Wooley, "A multichannel pipeline analog-to-digital converter for an integrated 3-D

ultrasound imaging system," *IEEE J. Solid-State Circuits*, vol. 38, no. 7, pp. 1266–1270, 2003.
[40] M. I. Fuller, K. Ranganathan, S. Zhou, T. N. Blalock, J. Hossack, and W. F. Walker, "Experimental system prototype of a portable, lowcost, c-scan ultrasound imaging device," *IEEE Trans. Biomed. Eng.*, vol. 55, no. 2, pp. 519–530, 2008.
[41] K. Hara, J. Sakano, M. Mori, S. Tamano, R. Sinomura, and K. Yamazaki, "A new 80 V 32 × 32ch low loss multiplexer LSI for a 3-D ultrasound imaging system," in *Proc. 17th Int. Symp. Power Semiconductor Devices and ICs*, 2005, pp. 359–362.
[42] L. Ye-Ming, R. Wodnicki, N. Chandra, and N. Rao, "An integrated 90 V switch array for medical ultrasound applications," in *2006 IEEE Custom Integrated Circuits Conf.*, 2006, pp. 269–272.
[43] I. Wygant, M. Karaman, O. Oralkan, and B. Khuri-Yakub, "Beamforming and hardware design for a multichannel front-end integrated circuit for real-time 3-D catheter-based ultrasonic imaging," in *SPIE Medical Imaging 2006*, vol. 6147, San Diego, CA, 2006.
[44] W. C. Black Jr. and D. N. Stephens, "CMOS chip for invasive ultrasound imaging," *IEEE J. Solid-State Circuits*, vol. 29, no. 11, pp. 1381–1387, 1994.
[45] E. D. Light, S. F. Idriss, P. D. Wolf, and S. W. Smith, "Real-time three-dimensional intracardiac echocardiography," *Ultrasound Med. Biol.*, vol. 27, no. 9, pp. 1177–1183, 2001.
[46] E. C. Pua, S. F. Idriss, P. D. Wolf, and S. W. Smith, "Real-time 3-D transesophageal echocardiography," *Ultrason. Imaging*, vol. 26, pp. 217–232, 2004.
[47] O. Oralkan, A. Ergun, J. Johnson, M. Karaman, U. Demirci, K. Kaviani, T. Lee, and B. Khuri-Yakub, "Capacitive micromachined ultrasonic transducers: Next-generation arrays for acoustic imaging?" *IEEE Trans. Ultrason. Ferroelectr. Freq. Control*, vol. 49, no. 11, pp. 1596–1610, 2002.
[48] D. M. Mills, "Medical imaging with capacitive micromachined ultrasound transducer (cMUT) arrays," in *2004 IEEE Ultrasonics Symp.*, vol. 1, 2004, pp. 384–390.
[49] D. T. Yeh, O. Oralkan, I. O. Wygant, M. O'Donnell, and B. T. Khuri-Yakub, "3-D ultrasound imaging using a forward-looking CMUT ring array for intravascular/intracardiac applications," *IEEE Trans. Ultrason. Ferroelectr. Freq. Control*, vol. 53, no. 6, pp. 1202–1211, 2006.
[50] O. Oralkan, S. T. Hansen, B. Bayram, G. G. Yaralioglu, A. S. Ergun, and B. T. Khuri-Yakub, "High-frequency CMUT arrays for high-resolution medical imaging," in *2004 IEEE Ultrasonics Symp.*, vol. 1, 2004, pp. 399–402.
[51] C.-H. Cheng, A. Ergun, and B. Khuri-Yakub, "Electrical through-wafer interconnects with 0.05 picofarads parasitic capacitance on 400 μm thick silicon substrates," in *Solid-State Sensor and Actuator Workshop*, Hilton Head Island, 2002.
[52] X. Zhuang, I. O. Wygant, D. S. Lin, M. Kupnik, O. Oralkan, and B. T. Khuri-Yakub, "Trench-isolated CMUT arrays with a supporting frame: Characterization and imaging results," in *2007 IEEE Ultrasonics Symp.*, 2007, pp. 507–510.
[53] M. Declerq, M. Schubert, and F. Clement, "5 V-to-75 V CMOS output interface circuits," in *1993 IEEE Int. Solid-State Circuits Conf.*, 1993, pp. 162–163, 283.
[54] A. Nikoozadeh, B. Bayram, G. Yaralioglu, and B. Khuri-Yakub, "Analytical calculation of collapse voltage of CMUT membrane [capacitive micromachined ultrasonic transducers]," in *2004 IEEE Ultrasonics Symp.*, vol. 1, 2004, pp. 256–259.
[55] I. Ladabaum, J. Xuecheng, H. T. Soh, A. Atalar, and B. T. Khuri-Yakub, "Surface micromachined capacitive ultrasonic transducers," *IEEE Trans. Ultrason. Ferroelectr. Freq. Control*, vol. 45, no. 3, pp. 678–690, 1998.
[56] A. Lohfink and P. C. Eccardt, "Linear and nonlinear equivalent circuit modeling of CMUTs," *IEEE Trans. Ultrason. Ferroelectr. Freq. Control*, vol. 52, no. 12, pp. 2163–2172, 2005.
[57] J. Graeme, *Photodiode Amplifiers: Op Amp Solutions*. New York: McGraw Hill, 1995.
[58] D. N. Stephens, K. K. Shung, J. Cannata, J. Zhao, R. Chia, H. Nguyen, K. Thomenius, A. Dentinger, D. G. Wildes, X. Chen, M. O'Donnell, R. I. Lowe, J. Pemberton, G. H. Burch, and D. J. Sahn, "Clinical application and technical challenges for intracardiac ultrasound imaging catheter based ICE imaging with EP mapping," in *2004 IEEE Ultrasonics Symp.*, vol. 1, 2004, pp. 772–777.
[59] A. S. Ergun, S. Barnes, and E. Gardner, "An assessment of the thermal efficiency of capacitive micromachined ultrasonic transducers," in *2007 IEEE Ultrasonics Symp.*, 2007, pp. 420–423.
[60] X. Zhuang, A. Nikoozadeh, M. Beasley, G. Yaralioglu, B. Khuri-Yakub, and B. L. Pruitt, "Biocompatible coatings for CMUTs in a harsh, aqueous environment," *J. Microelectromech. Syst.*, vol. 17, no. 5, pp. 994–1001, 2007.
[61] T. Misaridis and J. Jensen, "Use of modulated excitation signals in medical ultrasound. Part I: Basic concepts and expected benefits," *IEEE Trans. Ultrason. Ferroelectr. Freq. Control*, vol. 52, no. 2, pp. 177–191, 2005.

Ira O. Wygant received his B.S. degree in electrical engineering with a cross-college major in computer science from the University of Wyoming, Laramie, WY, in 1999. He received his M.S. degree in electrical engineering from Stanford University, Stanford, CA, in 2002 and his Ph.D in electrical engineering from Stanford University in 2008. After finishing his Ph.D, he joined National Semiconductor's research labs in Santa Clara, CA. His research interests include integrated circuit design, ultrasound imaging, and MEMs design and fabrication as they relate to capacitive micromachined ultrasound transducers.

Nafis Jamal received his B.S. degrees in electrical engineering and physics from Stanford University, Stanford, CA in 2008. He received his M.S. degree in electrical engineering from Stanford University in 2008 through the coterminal program. He is currently pursuing a Ph.D. degree in electrical engineering at Stanford University. Nafis has had internships with Sun Microsystems Labs. His research interests include ultrasound imaging and FPGA design for ultrasonic systems.

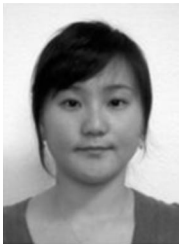

Hyunjoo J. Lee received the B.S. degree in Electrical Engineering and Computer Science and the M.Eng degree in Electrical Engineering, both from the Massachusetts Institute of Technology in 2004 and 2005, respectively. She is currently pursuing the Ph.D. degree in Electrical Engineering at Stanford University.

From 2004 to 2005, she was a MIT VI-A fellow at Analog Devices, Inc, Wilmington, MA, where she studied continuous-time signal-delta ADCs. In 2008, she was a student intern at National Semiconductor, Santa Clara, CA, where she developed an oscillator circuit that interfaces with a capacitive micromachined ultrasonic transducer (CMUT) for chemical sensing. Her research interests include sensor interface circuit design and bio/chemical sensor design. She is a member of the Eta Kappa Nu and Tau Beta Pi honor societies.

Amin Nikoozadeh (S'03) received the B.S. degree from Sharif University of Technology, Tehran, Iran, in 2002 and the M.S. degree from Stanford University, Stanford, CA, in 2004, both in electrical engineering. He is currently pursuing the Ph.D. degree in electrical engineering at Stanford University. His research interests include medical ultrasound imaging, image-guided therapeutics, MEMS, and analog circuit design.

Ömer Oralkan received the B.S. degree from Bilkent University, Ankara, Turkey, in 1995, the M.S. degree from Clemson University, Clemson, SC, in 1997, and the Ph.D. degree from Stanford University, Stanford, CA, in 2004, all in electrical engineering. He joined the research staff at the E. L. Ginzton Laboratory of Stanford University in 2004 as an Engineering Research Associate. He was promoted to the rank of Senior Research Engineer in 2007. He also serves as an Adjunct Professor of Electrical Engineering at Santa Clara University, Santa Clara, CA. His past and present research interests include analog and digital circuit design, semiconductor device physics and fabrication, micromachined sensors and actuators, and medical imaging. His current research focuses on the design and implementation of integrated systems for catheter-based medical imaging applications, photoacoustic imaging, and chemical and biological sensor arrays. Dr. Oralkan has authored and co-authored over 100 publications and received the 2002 Outstanding Paper Award of the IEEE Ultrasonics, Ferroelectrics, and Frequency Control Society. He is a member of the IEEE.

Mustafa Karaman (S'88-M'93) received the BS degree from the Middle East Technical University (Ankara, Turkey) in 1986, and the MS and PhD degrees from Bilkent University (Ankara, Turkey), in 1988 and 1992, respectively, all in electrical and electronics engineering. He was a post-doctoral fellow in the Biomedical Ultrasonics Laboratory of the University of Michigan (Ann Arbor, MI) between 1993-94. He has worked at the BU (Ankara, Turkey) as an associate professor and served in founding the faculty of engineering. He was with the E.L. Ginzton Laboratory at Stanford University (Stanford, CA) as a visiting faculty between 2000-02. He is currently working as a professor in the Department of Electronics Engineering of Işık University (Istanbul, Turkey) since 2002.

He has authored over one hundred papers in refereed journals and conferences. He received the IEEE UFFC Society 2002 Outstanding Paper Award as a co-author, and the 1996 H. Tuğaç Foundation Research Award of TUBITAK of Turkey.

His research interests include signal processing, medical ultrasonic imaging, and integrated circuit design.

Butrus (Pierre) T. Khuri-Yakub is a Professor of Electrical Engineering at Stanford University, Stanford, CA. He received the B.S. degree from the American University of Beirut, the M.S. degree from Dartmouth College, Hanover, NH, and the Ph.D. degree from Stanford University, all in electrical engineering. He was a Research Associate (1975-1978) then Senior Research Associate (1978-1982) at the E. L. Ginzton Laboratory of Stanford University and was promoted to the rank of Professor of Electrical Engineering in 1982. His current research interests include medical ultrasound imaging and therapy, micromachined ultrasonic transducers, smart biofluidic channels, microphones, ultrasonic fluid ejectors, and ultrasonic nondestructive evaluation, imaging and microscopy. He has authored over 450 publications and has been principal inventor or co-inventor of 78 U.S. and International issued patents. He was awarded the Medal of the City of Bordeaux in 1983 for his contributions to Nondestructive Evaluation, the Distinguished Advisor Award of the School of Engineering at Stanford University in 1987, the Distinguished Lecturer Award of the IEEE UFFC society in 1999, a Stanford University Outstanding Inventor Award in 2004, and a Distinguished Alumnus Award of the School of Engineering of the American University of Beirut in 2005.